Bloch waves at the surface of a single-layer coating D-shaped photonic crystal fiber

ESTEBAN GONZALEZ-VALENCIA[1], IGNACIO DEL VILLAR[2,3], AND PEDRO TORRES[1,*]

[1] Escuela de Física, Universidad Nacional de Colombia - Sede Medellín, A.A. 3840, Medellín, Colombia
[2] Institute of Smart Cities (ISC), Public University of Navarra, 31006 Pamplona, Spain
[3] Electrical and Electronic Engineering Department, Public University of Navarra, 31006 Pamplona, Spain
[*] Corresponding author: pitorres@unal.edu.co

Compiled March 28, 2020

Bloch surface wave (BSW) platforms are particularly interesting for light confinement and surface sensitivity, as an alternative to the metal-based surface plasmon polaritons (SPP). However, most of the reported BSW platforms require depositing a large number of alternating dielectric layers to realize the excitation of the surface waves. In this letter, we demonstrate an experimentally feasible D-shaped photonic crystal fiber (PCF) platform consisting of only a single dielectric layer on its flat surface, which can sustain Bloch waves at the boundary between the dielectric layer and the PCF cladding. The presence of the dielectric layer modifies the local effective refractive index, enabling a direct manipulation of the BSWs. In addition, the D-shaped structure provide direct contact with the external medium for sensing applications with an ultrahigh sensing figure-of-merit (1565 RIU^{-1}) and has the potential to be used over a wide range of analyte refractive index. © 2020 Optical Society of America

http://dx.doi.org/10.1364/ao.XX.XXXXXX

Bloch surface waves (BSWs) are electromagnetic surface waves excited at the interface between a homogeneous dielectric medium and an abruptly terminated photonic crystal (PC), typically a periodic dielectric multilayer, often referred to as one-dimensional PC (1DPC) or Bragg reflector [1]. Such dielectric PCs can be prepared virtually loss free, whereby BSWs can operate within a broad range of wavelengths with reduced spectral width compared to surface plasmons (SPPs) [2–5].

BSWs are either TE- or TM-polarized modes that can be obtained at any wavelength by suitably changing the geometry and materials of the PC [6]. These modes are confined near the surface of the structure and propagate along the boundary between the PC and the homogeneous dielectric with exponentially decaying field on both sides of the boundary [3, 4, 6]. Their confinement is due to total internal reflection from the side of the homogeneous dielectric and to the photonic band gap in the PC [7, 8]. Thus, the BSW dispersion relation below the light line of the homogeneous dielectric, and within the photonic band gap [9, 10].

Because the surface waves can increase the electromagnetic field enhancement at the surface, BSWs are appealing for amplifying the interaction between light and the materials deposited on the sample surface [8, 11–15], and thus they have been mainly exploited in biosensing [2, 3, 16, 17] and photonic devices [18, 19].

The typical platform used to excite this kind of surface waves employs the well-known Kretschmann-Raether prism-coupled configuration in order to realize the appropriate phase-matching conditions so that an incident light has a wave vector equal to the BSW [3, 6]. This excitation is detected by a reflectance dip in the angular or wavelength spectrum [2, 3, 16, 17], a change in intensity at a single wavelength [16, 20] or a variation in the phase properties of the reflected light [21, 22].

Recently, fiber optic with dielectric multilayer structures have been reported where BSWs can be excited [23–25], including configurations in which multilayer structures have been deposited on a tapered fiber [23], on the outer surface of optical fiber [24], or at the tip of a single-mode fiber [25]. More recently, we proposed a dielectric multilayer structure deposited inside a suspended-core photonic crystal fiber (PCF), where BSWs can be excited through the evanescent field of the core-guided fundamental mode [26]. We showed that the surface mode dispersion depends strongly on the termination of the 1DPC. In addition, using this approach, we designed a PCF refractive index (RI) sensor based on BSW resonance in the near infrared that can operate in an wide RI range, from 1.0 to 1.4, with a high 669 RIU^{-1} sensing figure-of-merit [26].

Different from the fiber optic one-dimensional multilayer dielectric structures reported in the literature, in this letter we demonstrate a PCF platform with a single layer that can sustain TE- and TM-polarized BSWs. The PCF structure is shown schematically in Fig. 1. It consists of a D-shaped profile of a solid-core PCF (SC-5.0-1040, NKT Photonics) to demonstrate its experimental feasibility. The D-shaped structure can be fabricated by using the side polishing technique [27], leaving two air-hole rows between the flat surface and the PCF core in order to ensure coupling conditions between these two regions [28]. The air-hole periodic microstructure which constitutes the PCF cladding is a two-dimensional triangular PC (2DPC) with a lattice constant $a = 3.1\,\mu m$, formed by circular air holes of diameter $d = 1.61\,\mu m$ in pure silica glass, resulting in diameter-

to-lattice ratio (d/a) of 0.52. Because the existence of surface modes depends strongly on the location of the PC termination, the D-shaped profile with an additional dielectric layer on its flat surface leads to a clear modification of the boundary conditions, which results in the creation of surface modes that satisfy these conditions [29]. At this point, it is worth noting that in some air-core photonic-bandgap fibers (PBFs), surface modes have been found, which are defect modes that form at the boundary between the air core and the photonic-crystal cladding, imposing serious limitations to air-core modes [30]. In our case, the novelty of our design is that the presence of the additional dielectric layer enables a direct manipulation of the surface modes, which are induced at the boundary between the additional dielectric layer and the photonic-crystal cladding, whereby the excitation wavelength of surface wave can be adjusted by choosing the thickness of this layer. In addition, the D-shaped structure provide direct contact with the surrounding medium for sensing applications and photonic devices.

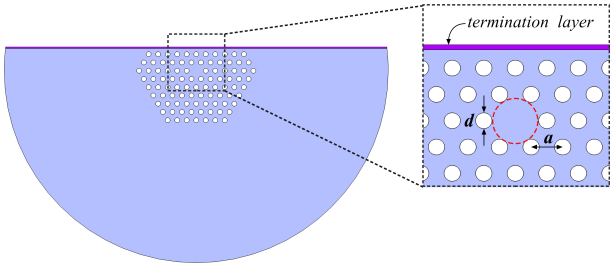

Fig. 1. (Color online) Schematic showing the D-shaped solid-core triangular PCF with a termination dielectric layer on its flat surface where Bloch waves can be excited by the evanescent field of the core-guided mode. The red dashed circle highlight the PCF core.

We consider the D-shaped triangular PCF with a termination layer of TiO_2, which enables a high index contrast with silica and, consequently, sharper BSW resonances [26]. Theoretical simulations were performed using the commercial software package FIMMWAVE, where silica and titanium oxide refractive indexes were calculated using the Sellmeier equation with the coefficients reported in [31] and [32], respectively. The titanium oxide extinction coefficient $\kappa_{TiO_2} = 4 \times 10^{-4}$ was taken from [33], while the pure silica extinction coefficient was neglected.

Similar to the prism-based BSW excitation, the fiber-based BSW can be efficiently excited as long as the effective index of the core-guided mode coincides with that of the BSW. As shown in Figs. 2(a) and 2(b), the D-shaped triangular PCF platform can sustain Bloch waves at the boundary between the termination layer and the PCF cladding, and their phase-matching conditions indicate that Bloch waves can be excited and the power of the light can be efficiently transferred from the fiber core to the 2DPC. Such phase-matching points differ for the TE-polarized light and TM-polarized light. The phase-matching for TE-polarized light is localized at 1277.6 (TE-BSW1), 1262.2 (TE-BSW2), 1236.2 (TE-BSW3), 1204.2 *nm* (TE-BSW4), whereas for TM-polarized light the phase-matching is located at 1275.9 (TM-BSW1), 1264 (TM-BSW2), 1242.3 (TM-BSW3), 1214.4 *nm* (TM-BSW4). The electric field distributions in Fig. 2, near the region of 2DPC at the resonant wavelength, show that a portion of the field is localized in the 2DPC for both polarizations, and the evanescent field of the BSWs penetrates the outer medium on top of the structure, which could be applied for sensing applications. When the light is transferred from the fiber core to 2DPC structure, a portion of it will be absorbed by the termination layer. In addition, if the layer length is long enough the light will eventually recouple to the fiber core; however, it will not happen for the selected D-shaped section length. As a combination of these two conditions, a loss peak at the resonant wavelength will appear at the transmission spectrum of the core-guided fundamental mode. As shown in Fig. 2 (blue lines), the loss peaks caused by the excitation of BSWs can be observed, which are consistent with the wavelengths of the BSW excitation analyzed by the dispersion curves.

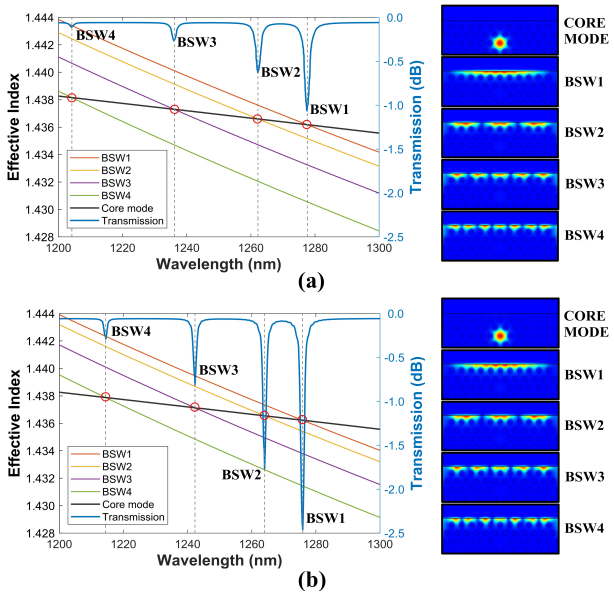

Fig. 2. (Color online) Dispersion curves (dashed lines), core-guided mode transmission spectra (blue lines) and electric-field distributions of the excited BSW modes for a 15 *mm* long D-shaped PCF BSW platform, assuming air as surrounding medium and a TiO_2 termination-layer thickness of **(a)** 50 *nm* for the TE-BSW modes and **(b)** 134 *nm* for the TM-BSW modes. The red circles highlight the phase-matching points.

The termination of 2DPCs is critical for the BSW excitation [29]. In our structure, for a high RI termination, the BSW field is more tightly confined to the surface and the associated surface mode shifts toward longer wavelengths as the termination layer is increased gradually (see Fig. 3). This demonstrates that the position of the surface wave resonance in this novel BSW platform can be tuned by changing the termination-layer thickness. However, the TE-BSW1 mode, being more confined in the TiO_2 layer, as evidenced from the field distributions in the insets of the Fig. 3, shifts more quickly than the TM-BSW1. The structure can sustain Bloch waves from the visible region with a termination-layer thickness of 10 *nm* to the mid-infrared (MIR) region with a termination-layer thickness of 106.6 *nm* (MIR spectroscopy enables the determination of characteristic vibrational resonances of many functional molecules and it can be used for label-free sensing, medical diagnostics, and food analysis [4]). Smaller termination-layer thicknesses were not considered since BSWs would be excited at wavelengths in which higher order modes can be propagated in the PCF core.

When the surrounding medium is changed, the evanescent

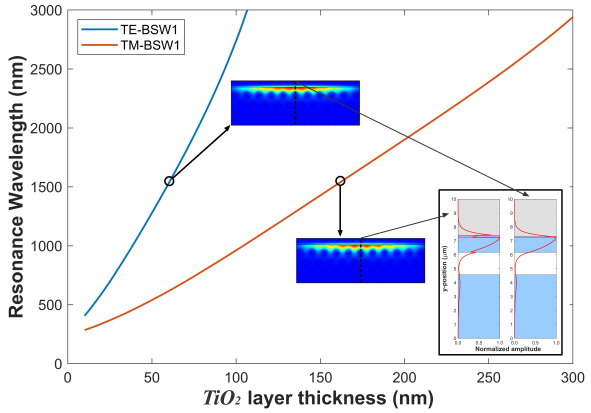

Fig. 3. (Color online) Spectral position of the BSW1 resonance wavelength as a function of the TiO_2 layer thickness for the TE modes (blue line) and TM modes (red line). Figure insets correspond to the electric-field distributions of the excited TE-BWS1 and TM-BSW1 modes. The profiles of the electric field along the dashed vertical line in the center of the fiber are shown in the lower right corner.

field of the BSW will be affected and thereby the phase matching condition will be altered. In order to study the RI sensing response of the single-layer coating D-shaped PCF platform, the transmission spectra under different surrounding RIs for TE- and TM-polarized light were calculated. As an example, Figs. 4(a) and 4(b) show results for two 15 mm long sensing structures with different termination layer thickness operating in the same spectral range. To this purpose, for the case of TE-polarized light a thickness for the TiO_2 layer of 50 nm while for TM-polarized light a thickness of 134 nm were respectively selected (see Fig. 3). These thicknesses were chosen so that the BSW1 resonances for both polarizations were excited at the same wavelength for a surrounding RI $n_s = 1.0$. As expected from our previous results (see Fig. 2), the four resonance peaks are very sharp and move towards longer wavelengths as the surrounding RI increases. It should also be noted that with the increase in the resonance wavelength, the loss of the core-guided mode gradually increases, because the effective RI difference between the core-guided mode and the BSW mode is reduced with the redshift of the resonance peaks, which eventually strengthens the coupling between the core guided mode and the BSW mode and therefore increases the loss of the core-guided mode. At this point, it is worth noting that the energy transferred from the core-guided mode to a BSW mode is a function of the length of the structure, which in this case leads to a higher coupling efficiency for the TE-BSW1 and TM-BSW2 modes.

In comparison with our previous BSW platform based on a one-dimensional multilayer structure deposited inside a three-hole suspended-core PCF [26], where some BSW modes can be excited in a relatively narrow wavelength range, which may cause neighboring loss peaks to overlap, forming a relatively wide peak, in this new platform the resonance peaks are very narrow and sufficiently separated from neighboring peaks to be able to differentiate them and, therefore, paves the way to develop sensors with improved characteristics. A more comprehensive description of the sensing response of the new structure can be seen in Fig. 4(c), which shows the wavelength shift of the BSW1 resonant peak as a function of surrounding RI for different polarization light. Considering the wavelength sensitivity, the BSW1 resonance peak is more suitable for RI sensing [26]. As can be seen in this figure, the sensing response exhibits a nonlinear feature which, as already explained, is due to the wavelength-dependent mode coupling between the core-guided mode and the BSW mode. Resonance shifts of $\Delta\lambda = 540\,nm$ and $\Delta\lambda = 422\,nm$ for TE-polarized light and TM-polarized

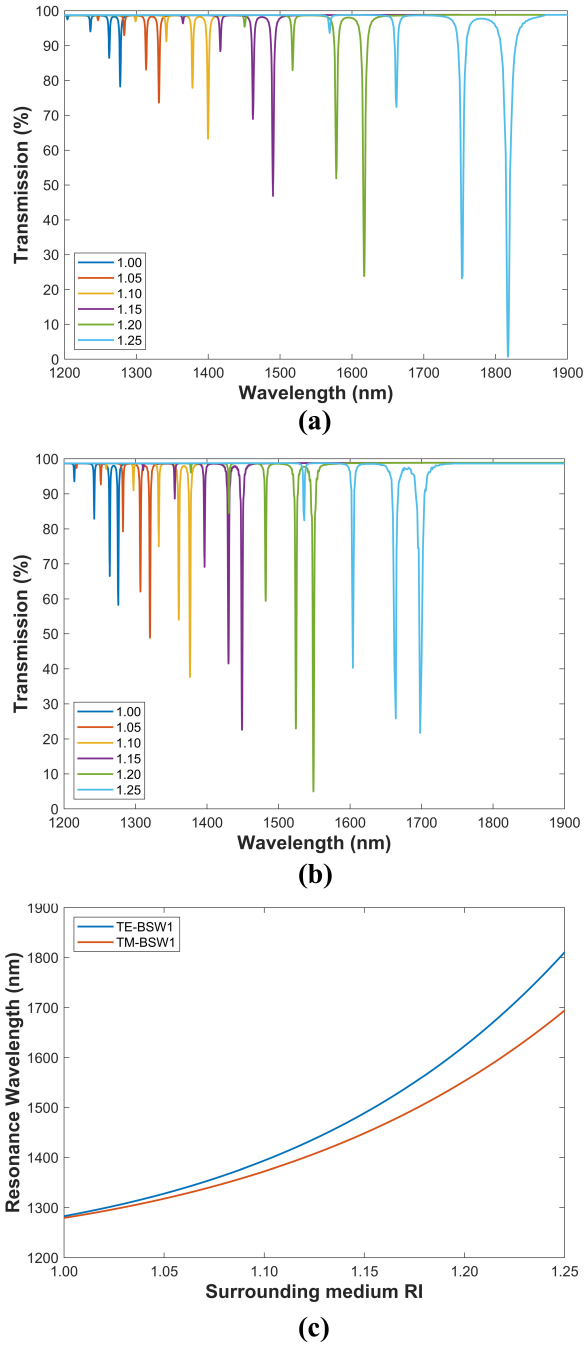

Fig. 4. (Color online) Spectral response of two 15 mm long BSW sensing structures based on single-layer coating D-shaped PCF operating in the same spectral range for **(a)** TE-polarized light with a 50 nm TiO_2 layer and **(b)** TM-polarized polarized light with a 134 nm TiO_2 layer. **(c)** BSW1 resonant peak as a function of surrounding refractive index for different polarization light.

light, respectively, were found for a surrounding RI change of $\Delta n_s = 0.25$. Table 1 summarizes the sensing response of the simulated structures near two representative surrounding RIs. The sensitivity is defined as $S_n = \partial\lambda/\partial n_s$, where λ is the BSW resonant wavelength. The sensitivities near $n_s = 1.25$ of this novel platform are much higher than that of other fiber based BSW platforms reported recently, for example, 2575 nm/RIU in [26] and 1900 nm/RIU in [23]. On the other hand, the figure of merit (FOM) is used to estimate the sensing performance [34]. The FOM is defined as FOM = Sn/FWHM, where FWHM is full width at half maximum. The resulting values near $n_s = 1.25$ represent, to the best our knowledge, the highest FOM achieved by optical sensors based on surface waves.

Table 1. Comparison of the sensing response of the simulated structures in Fig. 4

n_s	Resonance	FWHM	Sensitivity	FOM
		nm	nm/RIU	RIU^{-1}
1.00	TE-BSW1	2.18	735	337
	TM-BSW1	1.52	640	421
1.25	TE-BSW1	5.58	5492	984
	TM-BSW1	2.61	4085	1565

In conclusion, we have theoretically demonstrated a novel approach for BSW excitation based on D-shaped triangular PCF. By exploiting the air-hole periodic microstructure of the PCF cladding, the BSW platform can be realized with only a single high RI dielectric layer on its flat surface. Moreover, BSW excitation was demonstrated in the visible range to MIR with a termination layer of TiO_2 by tuning the thickness of the termination layer. Due to the high sensitivity to the surrounding medium, this PCF-based BSW platform could be exploited for refractive index sensing. Moreover, in view of the high FOM of the sensor, it could be used in the domain of biological or chemical sensor, where this parameter is especially important.

FUNDING INFORMATION

This work was supported in part by the Universidad Nacional de Colombia, Hermes code 46509, and in part by the Spanish Agencia Estatal de Investigacion (AEI) and European Regional Development Fund (FEDER) (TEC2016-78047-R). E.G.V. acknowledges the support of COLCIENCIAS through the Doctoral Scholarship program.

DISCLOSURES

The authors declare no conflicts of interest.

REFERENCES

1. P. Yeh, A. Yariv, and A. Y. Cho, Appl. Phys. Lett. **32**, 104 (1978).
2. M. Shinn and W. M. Robertson, Sensors Actuators, B: Chem. **105**, 360 (2005).
3. A. Sinibaldi, N. Danz, E. Descrovi, P. Munzert, U. Schulz, F. Sonntag, L. Dominici, and F. Michelotti, Sensors Actuators, B: Chem. **174**, 292 (2012).
4. C. Z. Deng, Y. L. Ho, Y. C. Lee, Z. Wang, Y. H. Tai, M. Zyskowski, H. Daiguji, and J. J. Delaunay, Appl. Phys. Lett. **115** (2019).
5. M. Liscidini and J. E. Sipe, Appl. Phys. Lett. **91**, 253125 (2007).
6. M. U. Khan and B. Corbett, Sci. Technol. Adv. Mater. **17**, 398 (2016).
7. J. D. Joannopoulos, S. G. Johnson, J. N. Winn, and R. D. Meade, *Photonic crystals: Molding the flow of light* (Princeton University Press, 2008), 2nd ed.
8. S. Pirotta, M. Patrini, M. Liscidini, M. Galli, G. Dacarro, G. Canazza, G. Guizzetti, D. Comoretto, and D. Bajoni, Appl. Phys. Lett. **104**, 13 (2014).
9. Y. Li, T. Yang, Z. Pang, G. Du, S. Song, and S. Han, Opt. Express **22**, 21403 (2014).
10. W. M. Robertson and M. S. May, Appl. Phys. Lett. **74**, 1800 (1999).
11. T. Kovalevich, D. Belharet, L. Robert, M.-S. Kim, H. P. Herzig, T. Grosjean, and M.-P. Bernal, Photonics Res. **5**, 649 (2017).
12. M. Menotti and M. Liscidini, J. Opt. Soc. Am. B **32**, 431 (2015).
13. A. Delfan, M. Liscidini, and J. E. Sipe, J. Opt. Soc. Am. B **29**, 1863 (2012).
14. M. Ballarini, F. Frascella, F. Michelotti, G. Digregorio, P. Rivolo, V. Paeder, V. Musi, F. Giorgis, and E. Descrovi, Appl. Phys. Lett. **99**, 043302 (2011).
15. M. Liscidini, M. Galli, M. Shi, G. Dacarro, M. Patrini, D. Bajoni, and J. E. Sipe, Opt. Lett. **34**, 2318 (2009).
16. A. Farmer, A. C. Friedli, S. M. Wright, and W. M. Robertson, Sensors Actuators, B: Chem. **173**, 79 (2012).
17. F. Giorgis, E. Descrovi, C. Summonte, L. Dominici, and F. Michelotti, Opt. Express **18**, 8087 (2010).
18. A. Angelini, E. Barakat, P. Munzert, L. Boarino, N. De Leo, E. Enrico, F. Giorgis, H. P. Herzig, C. F. Pirri, and E. Descrovi, Sci. Reports **4**, 1 (2014).
19. L. Yu, E. Barakat, T. Sfez, L. Hvozdara, J. Di Francesco, and H. P. Herzig, Light. Sci. Appl. **3** (2014).
20. W. Kong, Z. Zheng, Y. Wan, S. Li, J. Liu, Z. Zheng, X. Zhao, Y. Liu, Y. Bian, Y. Wan, S. Li, and J. Liu, Sensors Actuators, B: Chem. **193**, 467 (2014).
21. Y. Li, T. Yang, S. Song, Z. Pang, G. Du, and S. Han, Appl. Phys. Lett. **103** (2013).
22. A. Sinibaldi, R. Rizzo, G. Figliozzi, E. Descrovi, N. Danz, P. Munzert, A. Anopchenko, and F. Michelotti, Opt. Express **21**, 23331 (2013).
23. T. Tu, F. Pang, S. Zhu, J. Cheng, H. Liu, J. Wen, and T. Wang, Opt. Express **25**, 9019 (2017).
24. X.-J. Tan and X.-S. Zhu, Opt. Express **24**, 16016 (2016).
25. M. Scaravilli, A. Micco, G. Castaldi, G. Coppola, M. Gioffrè, M. Iodice, V. La Ferrara, V. Galdi, and A. Cusano, Adv. Opt. Mater. **6**, 1 (2018).
26. E. Gonzalez-Valencia, R. Acuna Herrera, and P. Torres, Opt. Express **27**, 8236 (2019).
27. T. Wu, Y. Shao, Y. Wang, S. Cao, W. Cao, F. Zhang, C. Liao, J. He, Y. Huang, M. Hou, and Y. Wang, Opt. Express **25**, 20313 (2017).
28. P. Torres, E. Reyes-Vera, A. Díez, and M. V. Andrés, Opt. Lett. **39**, 1593 (2014).
29. F. Ramos-Mendieta and P. Halevi, Phys. Rev. B - Condens. Matter Mater. Phys. **59**, 15112 (1999).
30. M. J. F. Digonnet, H. K. Kim, J. Shin, S. Fan, and G. S. Kino, Opt. Express **12**, 1864 (2004).
31. B. E. A. Saleh and M. C. Teich, *Fundamentals of photonics* (Wiley, 2007), 2nd ed.
32. J. R. DeVore, J. Opt. Soc. Am. **41**, 416 (1951).
33. Y. Wan, Z. Zheng, W. Kong, Y. Liu, Z. Lu, and Y. Bian, Opt. Lett. **36**, 3539 (2011).
34. A. Urrutia, I. Del Villar, P. Zubiate, and C. R. Zamarreño, Laser Photonics Rev. **13**, 1 (2019).

FULL REFERENCES

1. P. Yeh, A. Yariv, and A. Y. Cho, "Optical surface waves in periodic layered media," Appl. Phys. Lett. **32**, 104–105 (1978).
2. M. Shinn and W. M. Robertson, "Surface plasmon-like sensor based on surface electromagnetic waves in a photonic band-gap material," Sensors Actuators, B: Chem. **105**, 360–364 (2005).
3. A. Sinibaldi, N. Danz, E. Descrovi, P. Munzert, U. Schulz, F. Sonntag, L. Dominici, and F. Michelotti, "Direct comparison of the performance of Bloch surface wave and surface plasmon polariton sensors," Sensors Actuators, B: Chem. **174**, 292–298 (2012).
4. C. Z. Deng, Y. L. Ho, Y. C. Lee, Z. Wang, Y. H. Tai, M. Zyskowski, H. Daiguji, and J. J. Delaunay, "Two-pair multilayer Bloch surface wave platform in the near-and mid-infrared regions," Appl. Phys. Lett. **115** (2019).
5. M. Liscidini and J. E. Sipe, "Enhancement of diffraction for biosensing applications via Bloch surface waves," Appl. Phys. Lett. **91**, 253125 (2007).
6. M. U. Khan and B. Corbett, "Bloch surface wave structures for high sensitivity detection and compact waveguiding," Sci. Technol. Adv. Mater. **17**, 398–409 (2016).
7. J. D. Joannopoulos, S. G. Johnson, J. N. Winn, and R. D. Meade, *Photonic crystals: Molding the flow of light* (Princeton University Press, 2008), 2nd ed.
8. S. Pirotta, M. Patrini, M. Liscidini, M. Galli, G. Dacarro, G. Canazza, G. Guizzetti, D. Comoretto, and D. Bajoni, "Strong coupling between excitons in organic semiconductors and Bloch surface waves," Appl. Phys. Lett. **104**, 13–16 (2014).
9. Y. Li, T. Yang, Z. Pang, G. Du, S. Song, and S. Han, "Phase-sensitive Bloch surface wave sensor based on variable angle spectroscopic ellipsometry," Opt. Express **22**, 21403 (2014).
10. W. M. Robertson and M. S. May, "Surface electromagnetic wave excitation on one-dimensional photonic band-gap arrays," Appl. Phys. Lett. **74**, 1800–1802 (1999).
11. T. Kovalevich, D. Belharet, L. Robert, M.-S. Kim, H. P. Herzig, T. Grosjean, and M.-P. Bernal, "Experimental evidence of Bloch surface waves on photonic crystals with thin-film LiNbO3 as a top layer," Photonics Res. **5**, 649 (2017).
12. M. Menotti and M. Liscidini, "Optical resonators based on Bloch surface waves," J. Opt. Soc. Am. B **32**, 431–438 (2015).
13. A. Delfan, M. Liscidini, and J. E. Sipe, "Surface enhanced Raman scattering in the presence of multilayer dielectric structures," J. Opt. Soc. Am. B **29**, 1863 (2012).
14. M. Ballarini, F. Frascella, F. Michelotti, G. Digregorio, P. Rivolo, V. Paeder, V. Musi, F. Giorgis, and E. Descrovi, "Bloch surface waves-controlled emission of organic dyes grafted on a one-dimensional photonic crystal," Appl. Phys. Lett. **99**, 043302 (2011).
15. M. Liscidini, M. Galli, M. Shi, G. Dacarro, M. Patrini, D. Bajoni, and J. E. Sipe, "Strong modification of light emission from a dye monolayer via Bloch surface waves," Opt. Lett. **34**, 2318 (2009).
16. A. Farmer, A. C. Friedli, S. M. Wright, and W. M. Robertson, "Biosensing using surface electromagnetic waves in photonic band gap multilayers," Sensors Actuators, B: Chem. **173**, 79–84 (2012).
17. F. Giorgis, E. Descrovi, C. Summonte, L. Dominici, and F. Michelotti, "Experimental determination of the sensitivity of Bloch Surface Waves based sensors," Opt. Express **18**, 8087 (2010).
18. A. Angelini, E. Barakat, P. Munzert, L. Boarino, N. De Leo, E. Enrico, F. Giorgis, H. P. Herzig, C. F. Pirri, and E. Descrovi, "Focusing and extraction of light mediated by Bloch surface waves," Sci. Reports **4**, 1–9 (2014).
19. L. Yu, E. Barakat, T. Sfez, L. Hvozdara, J. Di Francesco, and H. P. Herzig, "Manipulating Bloch surface waves in 2D: A platform concept-based flat lens," Light. Sci. Appl. **3** (2014).
20. W. Kong, Z. Zheng, Y. Wan, S. Li, J. Liu, Z. Zheng, X. Zhao, Y. Liu, Y. Bian, Y. Wan, S. Li, and J. Liu, "High-sensitivity sensing based on intensity-interrogated Bloch surface wave sensors," Sensors Actuators, B: Chem. **193**, 467–471 (2014).
21. Y. Li, T. Yang, S. Song, Z. Pang, G. Du, and S. Han, "Phase properties of Bloch surface waves and their sensing applications," Appl. Phys. Lett. **103** (2013).
22. A. Sinibaldi, R. Rizzo, G. Figliozzi, E. Descrovi, N. Danz, P. Munzert, A. Anopchenko, and F. Michelotti, "A full ellipsometric approach to optical sensing with Bloch surface waves on photonic crystals," Opt. Express **21**, 23331 (2013).
23. T. Tu, F. Pang, S. Zhu, J. Cheng, H. Liu, J. Wen, and T. Wang, "Excitation of Bloch surface wave on tapered fiber coated with one-dimensional photonic crystal for refractive index sensing," Opt. Express **25**, 9019–9027 (2017).
24. X.-J. Tan and X.-S. Zhu, "Optical fiber sensor based on Bloch surface wave in photonic crystals," Opt. Express **24**, 16016–16026 (2016).
25. M. Scaravilli, A. Micco, G. Castaldi, G. Coppola, M. Gioffrè, M. Iodice, V. La Ferrara, V. Galdi, and A. Cusano, "Excitation of Bloch surface waves on an optical fiber tip," Adv. Opt. Mater. **6**, 1–10 (2018).
26. E. Gonzalez-Valencia, R. Acuna Herrera, and P. Torres, "Bloch surface wave resonance in photonic crystal fibers: Towards ultra-wide range refractive index sensors," Opt. Express **27**, 8236–8245 (2019).
27. T. Wu, Y. Shao, Y. Wang, S. Cao, W. Cao, F. Zhang, C. Liao, J. He, Y. Huang, M. Hou, and Y. Wang, "Surface plasmon resonance biosensor based on gold-coated side-polished hexagonal structure photonic crystal fiber," Opt. Express **25**, 20313 (2017).
28. P. Torres, E. Reyes-Vera, A. Díez, and M. V. Andrés, "Two-core transversally chirped microstructured optical fiber refractive index sensor," Opt. Lett. **39**, 1593–1596 (2014).
29. F. Ramos-Mendieta and P. Halevi, "Surface electromagnetic waves in two-dimensional photonic crystals: effect of the position of the surface plane," Phys. Rev. B - Condens. Matter Mater. Phys. **59**, 15112–15120 (1999).
30. M. J. F. Digonnet, H. K. Kim, J. Shin, S. Fan, and G. S. Kino, "Simple geometric criterion to predict the existence of surface modes in air-core photonic-bandgap fibers," Opt. Express **12**, 1864 (2004).
31. B. E. A. Saleh and M. C. Teich, *Fundamentals of photonics* (Wiley, 2007), 2nd ed.
32. J. R. DeVore, "Refractive indices of rutile and sphalerite," J. Opt. Soc. Am. **41**, 416 (1951).
33. Y. Wan, Z. Zheng, W. Kong, Y. Liu, Z. Lu, and Y. Bian, "Direct experimental observation of giant Goos – Hänchen shifts from bandgap-enhanced total internal reflection," Opt. Lett. **36**, 3539–3541 (2011).
34. A. Urrutia, I. Del Villar, P. Zubiate, and C. R. Zamarreño, "A Comprehensive review of optical fiber refractometers: Toward a standard comparative criterion," Laser Photonics Rev. **13**, 1–32 (2019).